ChemComm

Cite this: *Chem. Commun.*, 2011, **47**, 9849–9851

www.rsc.org/chemcomm

COMMUNICATION

Template free electrochemical deposition of ZnSb nanotubes for Li ion battery anodes†

Somaye Saadat,[a] Jixin Zhu,[a] Mohammad Mehdi Shahjamali,[a] Saeed Maleksaeedi,[c] Yee Yan Tay,[a] Bee Yen Tay,[c] Huey Hoon Hng,[a] Jan Ma[a] and Qingyu Yan*[abd]

Received 30th June 2011, Accepted 13th July 2011
DOI: 10.1039/c1cc13900b

ZnSb nanotubes were grown through a template free electrodeposition method under over-potential conditions. The growth of the nanotubes was attributed to the template effect from H_2 bubbles. Due to their hollow structure, the ZnSb nanotubes depicted better Li ion storage performance compared to that of ZnSb nanoparticles deposited under different conditions.

The lithium ion battery, as an effective electrochemical energy storage device, has attracted much interest recently.[1] Graphite has been widely used as the anode in commercial Li ion batteries, which showed stable cycling performance. However, the lithium intercalation into graphite occurs at potentials close to that of metallic Li deposition, which gives rise to serious safety issues.[2,3] Thus, the study on alternative electrode materials is still actively pursued. Sb-based intermetallic compounds are attractive anode materials with high theoretical capacities and higher Li intercalation potentials than those of graphite. Although increased anode potentials result in lower battery power, they insure safer applications.[4,5] However, in such materials, the volume expansion during the interaction with Li ions normally causes electrode pulverization and poor cycling stability.[6]

One effective strategy to achieve high reversible capacities is to prepare nanostructured electrodes with sufficient buffering space, *e.g.* porous,[5] one dimensional structures,[7] to alleviate the volume swings. These nanostructured electrodes also possess the advantage of large surface-to-volume ratio and short diffusion distance.[8] The synthesis of nanostructured materials is achieved by many techniques. Electrodeposition is an effective process as it is low-cost and energy-efficient. However, the preparation of nanostructures by this method normally requires hard templates.[9,10]

In a recent report,[4] ZnSb nanocrystallites embedded in amorphous carbon achieved 705 and 600 mA h g^{-1} charge and discharge capacities, and an initial coulombic efficiency of 85%. The ZnSb/C electrode maintained a capacity of 520 mA h g^{-1} even after 200 cycles demonstrating the superior electrochemical properties of this nanocomposite. Herein, we report a template free single-step synthesis process to prepare ZnSb nanotubes with adjustable morphology by electrodeposition under controlled over-potential conditions. The growth of the ZnSb nanotubes is believed to be initiated by the H_2 bubbles generated under such over-potential conditions. Such hollow nanostructures are advantageous as electrode materials for Li ion batteries to accommodate the large volume changes during the cycling process. The electrochemical tests showed that the ZnSb nanotubes exhibited low irreversible capacity loss (ICL), high specific capacities, satisfactory cycling performance and rate capability, which were better than those of ZnSb nanoparticles (NPs) deposited under different parameters.

Fig. 1A shows the scanning electron microscopy (SEM) images of Zn–Sb alloys grown on ITO glass from an ethylene glycol (EG) solution containing 0.05 mol L^{-1} $ZnCl_2$ and 0.03 mol L^{-1} $SbCl_3$ under a deposition voltage $V_d = -7$ V for 200 seconds (also see Fig. S1A in ESI†). The experimental detail is discussed in the experimental section in ESI.† It reveals that the as-deposited Zn–Sb alloy forms one dimensional (1D) nanostructure arrays on the substrate. The diameter and length of these Zn–Sb 1D nanostructures are in the range of 80–130 nm (indicated by arrows in Fig. 1A) and 1–1.5 μm, respectively. It is noted that some of the wires are branched. The transmission electron microscopy (TEM) image (Fig. 1B) shows that these 1D nanostructures are close-end nanotubes with shell thickness of 15–30 nm. The average atomic ratio as examined by EDX in TEM is Zn : Sb = 52 : 48. The high resolution (HR) TEM observation of the Zn–Sb nanotubes indicates that they are polycrystalline (see ESI†, Fig. S1C) with the grain size in the range of 5–10 nm. The HRTEM image and the fast Fourier transform pattern (see Fig. S1B in the ESI†) indicate that the deposits are hexagonal ZnSb (JCPDF 18-0140), which is also confirmed by the XRD result (Fig. 1F). Increasing the deposition time to 400 s led to a change in the morphology of the Zn–Sb nanotubes. The resulting Zn–Sb

[a] *School of Materials Science and Engineering, Nanyang Technological University, 50 Nanyang Avenue, Singapore 639798, Singapore. E-mail: alexyan@ntu.edu.sg; Fax: +65 67909081; Tel: +65 67904583*
[b] *TUM CREATE Centre for Electromobility, Singapore 637459*
[c] *Singapore Institute of Manufacturing Technology, 71 Nanyang Drive, Singapore 638075*
[d] *Energy research Institute @ NTU, zNanyang Technological University, Singapore 638075*

† Electronic supplementary information (ESI) available: Experimental details, SEM and TEM images of Zn–Sb nanotubes, SEM, TEM and XRD of ZnSb nanoparticles, schematic drawing of the ZnSb growth mechanism, charge/discharge voltage profile of ZnSb nanostructures. See DOI: 10.1039/c1cc13900b

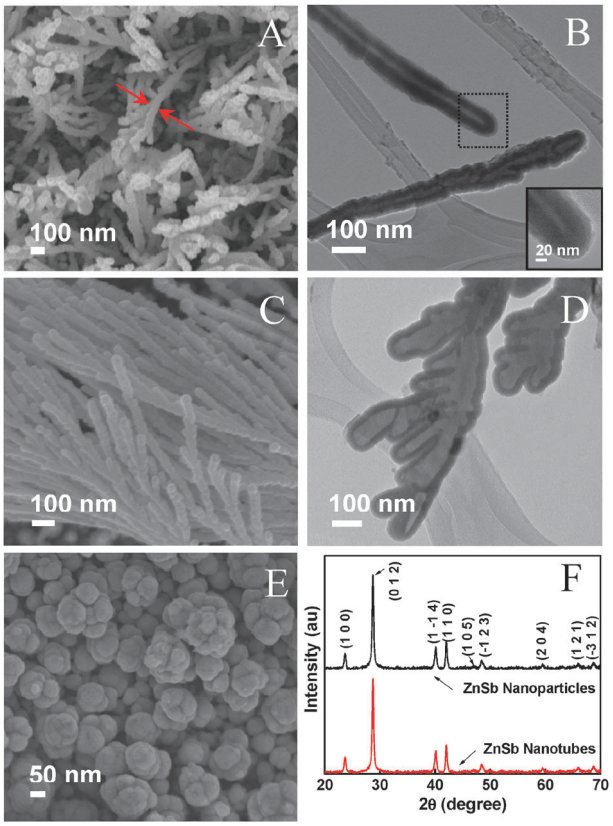

Fig. 1 SEM and TEM images of Zn–Sb nanotubes electrodeposited in EG solution with $I_{ZnCl_2-SbCl_3}$ = 1.6 and V_d = −7 V for (A and B) 200 s, (C and D) 400 s, (E) SEM image of Zn–Sb nanoparticles electrodeposited with $I_{ZnCl_2-SbCl_3}$ = 1.6 and V_d = −2 V for 200 s, (F) XRD pattern of ZnSb nanotubes and nanoparticles electrodeposited with $I_{ZnCl_2-SbCl_3}$ = 1.6, V_d = −7 and V_d = −2 V, respectively, for 200 s.

nanotubes are longer, *e.g.* 3 μm in length, with more branches (see Fig. 1C). The observed branches in the nanotubes also grew longer and larger, *e.g.* 0.5 μm in length and 50 nm in diameter. The TEM study reveals that the hollow structure is preserved (see Fig. 1D). Interestingly, when changing the deposition voltage to −9 V and keeping other deposition conditions the same, we found that the ZnSb nanotubes became open-end (see ESI†, Fig. S2A and B). Such open-end nanotubes are close packed with diameter of 70–110 nm and shell thickness of 15–25 nm. For comparison purpose, we also deposited Zn–Sb alloys with a lower voltage, *e.g.* −2 V, which led to the growth of NPs. The SEM (see Fig. 1E and also Fig. S3A in ESI†) and TEM images (see ESI†, Fig. S3B) reveal a relatively large size distribution of the Zn–Sb NPs, *e.g.* 20–100 nm. The average atomic ratio of NPs is Zn : Sb = 51 : 49 as indicated by the EDX measurement in TEM, which is similar to that of ZnSb nanotubes. The HRTEM observation shows that the Zn–Sb NPs are single crystalline (see ESI†, Fig. S3C) and the observed interfringe spacings of 0.3 nm and 0.26 nm correspond to the (102) and (103) planes of hexagonal ZnSb (JCPDF 18-0140), respectively (see ESI†, Fig. S3D). The XRD pattern of the ZnSb NPs (see Fig. 1F) also confirms the pure hexagonal ZnSb. Based on the above observation, the template-free formation of ZnSb nanotubes is possibly related to the bubble template effect[11] which is schematically illustrated in Fig.S4 in ESI.† Under over-potential conditions, *e.g.* −7–9 V, the used electrolyte (*e.g.* EG) goes through the following reaction:[12] $C_2H_6O_2 + 2e^- \Leftrightarrow H_2\uparrow + C_2H_6O_2^{2-}$, which can lead to the formation of H_2 bubbles on the cathode surfaces.[13] On the other hand, the reduction of metal ions occurs on the cathode surfaces simultaneously with the H_2 bubble evolution. The evolving H_2 bubbles suppress the reduction of metal ions while guiding their deposition in the vicinity of surfaces by acting as a dynamic template for the growth of nanotubes (see ESI†, Fig. S4). The polycrystalline nature of the ZnSb nanotubes is possibly due to the fast growth process which may lead to the generation of structural defects and in turn form grain boundaries. As the deposition process continues, the H_2 gas bubbles may split and cause the growth of branches (see ESI†, Fig. S4C and D). This is mainly concluded from the fact that the hollow space inside the branched nanotubes is well connected (see Fig. 1D). At a high deposition voltage, *e.g.* −9 V, the evolution of H_2 can be faster than deposition of metallic ions, which leads to the formation of open-end nanotubes (see the schematic drawing in Fig. S5 in ESI†).

To study the Li-ion storage properties of the ZnSb nanostructures, a series of electrochemical measurements were carried out based on the half-cell configuration (see details in the experimental section in ESI†).[5] The cyclic voltammograms (CVs) of the first and second cycles of ZnSb close-end nanotubes deposited with V_d = −7 V for 200 s are displayed in Fig. S6A (ESI†). The observed redox peaks in the charge and discharge cycles are in agreement with the previous report on ZnSb.[4] In this work, CNT was added as a conducting agent and the mass of ZnSb and CNT was considered as the active material. The theoretical capacity of the anode is calculated based on the theoretical capacity of ZnSb (570 mA h g^{-1}) and CNT (372 mA h g^{-1}), respectively, resulting in an electrode final capacity of 530 mA h g^{-1}. The corresponding charge/discharge voltage profiles of the ZnSb nanotubes at a current density of 100 mA g^{-1} (0.18 C) (see ESI†, Fig. S6B) showed an initial discharge capacity of 637 mA h g^{-1} and a subsequent charge capacity of 576 mA h g^{-1}, resulting in a low ICL of 10%. ZnSb NPs exhibited a lower initial specific discharge capacity of 550 mA h g^{-1} and a subsequent charge capacity of 485 mA h g^{-1}, which resulted in an ICL of 10%. The extra discharge capacity of the ZnSb anode may be attributed to the larger electrochemical active surface area of CNT and/or grain boundary area of the nanocrystallized ZnSb and the cumulative effect of ZnSb and CNT.[14,15] It is worth to point out that such a low irreversible capacity loss (ICL) is highly desired for full cell assembling. Anode materials with high ICL and high irreversible capacity require extra cathode materials in the battery cell, which increases the fabrication cost and reduces the total energy density. The charge/discharge cycling performance of the ZnSb nanotubes deposited with V_d = −7 V was evaluated at a current density of 100 mA g^{-1} (0.18 C) (see Fig. 2A). With a discharge capacity of 621 mA h g^{-1} during the second cycle, the ZnSb nanotubes maintained a discharge capacity of 400 mA h g^{-1} with a columbic efficiency of 98% during the 100th cycle. Such a specific capacity value of ZnSb nanotubes after 100 cycles is higher than the theoretical capacity of commercially used graphite anodes, *e.g.* 372 mA h g^{-1}.

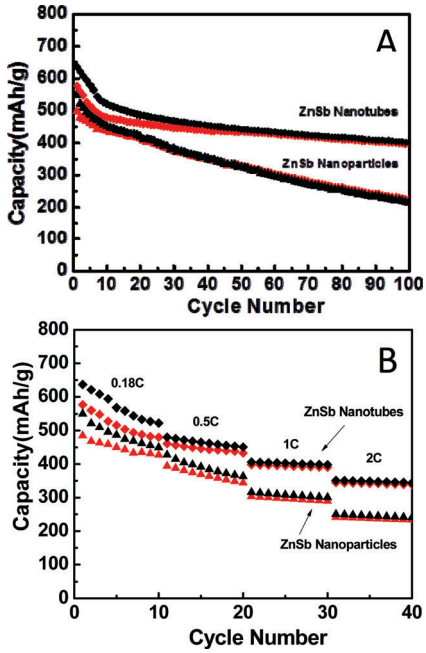

Fig. 2 (A) Charge/discharge cycling performance of ZnSb nanotubes and nanoparticles between 0–2 V (*vs.* Li/Li^+) at a current density of 100 mA g^{-1} (0.18 C), (B) plot of the discharge and charge capacity *vs.* cycle number for the ZnSb nanotube and nanoparticle electrodes at various C rates (ZnSb: 1 C 570 mA h g^{-1}, CNT: 1 C 372 mA h g^{-1}).

Moreover, considering the potential safer operation for Li-ion batteries, the ZnSb nanotubes produced in this study are attractive for anode applications. The electrochemical performance of open end and close end nanotubes is compared in Fig S7 in ESI.† It was observed that the performance is similar. The charge/discharge cycling performance of the ZnSb NPs was also investigated. ZnSb nanotubes as compared to ZnSb NPs depicted a lower discharge capacity of 521 mA h g^{-1} at 0.18 C during the second cycle, which decreased rapidly to 215 mA h g^{-1} in the 100th cycle. The higher initial capacities obtained in the ZnSb nanotubes as compared to those of NPs are possibly due to their open structure resulting in improved ion diffusion. The stable performance of ZnSb nanotubes is mainly attributed to their 1D morphology and hollow structure, which provides additional 'buffer' space to accommodate the generated strain during cycling.[16] Additionally, the influence of CNT was studied by comparing the battery performance of ZnSb nanotubes with a CNT free ZnSb nanotube electrode (see Fig. S8 in ESI†) which showed higher initial capacity due to higher theoretical capacity and slightly poorer capacity retention. The rate capability of ZnSb nanotube and nanoparticle electrodes was also tested (Fig. 2B). At different C rates, ZnSb nanotubes delivered higher specific capacities than those of ZnSb nanoparticles. The ZnSb nanotubes depicted specific capacities of 406 and 350 mA h g^{-1} at 1 C and 2 C, respectively, which were 22% and 30% higher than those of ZnSb nanoparticles.

In summary, ZnSb nanotubes with tuneable morphology were grown by a template-free electrochemical deposition process under over-potential conditions. Such a growth process of a tubular structure is believed to be initiated by the H_2-bubble-template effect under highly over-potential conditions. The electrochemical tests revealed that these ZnSb nanotubes exhibited low ICL, which is desired for applications as anode materials for full Li ion battery cells. Also, the ZnSb nanotubes showed higher Li ion storage capacities and satisfactory cyclability and rate capability as compared to those of ZnSb NPs deposited under different conditions. The better Li storage performance of the ZnSb nanotubes is mainly attributed to their hollow and one dimensional nanostructure, which can facilitate the Li ion diffusion and buffer the strain induced by the volume expansion during the lithiation process.

The authors gratefully acknowledge AcRF Tier 1 RG 31/08 of MOE (Singapore), NRF2009EWT-CERP001-026 (Singapore), Singapore Ministry of Education (MOE2010-T2-1-017), A*STAR SERC grant 1021700144 and Singapore MPA 23/04.15.03 grand.

Notes and references

1 J. M. Tarascon and M. Armand, *Nature*, 2001, **414**, 359–367.
2 R. Fong, U. von Sacken and J. R. Dahn, *J. Electrochem. Soc.*, 1990, **137**, 2009–2013.
3 P. G. Bruce, B. Scrosati and J. M. Tarascon, *Angew. Chem., Int. Ed.*, 2008, **47**, 2930–2946.
4 C. M. Park and H. J. Sohn, *Adv. Mater.*, **22**, 47–52.
5 S. Saadat, Y. Y. Tay, J. Zhu, P. F. Teh, S. Maleksaeedi, M. M. Shahjamali, M. Shakerzadeh, M. Srinivasan, B. Y. Tay, H. H. Hng, J. Ma and Q. Yan, *Chem. Mater.*, 2011, **23**, 1032–1038.
6 M. Winter, J. O. Besenhard, M. E. Spahr and P. Novák, *Adv. Mater.*, 1998, **10**, 725–763.
7 C. K. Chan, H. Peng, G. Liu, K. McIlwrath, X. F. Zhang, R. A. Huggins and Y. Cui, *Nat. Nanotechnol.*, 2008, **3**, 31–35.
8 A. S. Aricò, P. Bruce, B. Scrosati, J. M. Tarascon and W. Van Schalkwijk, *Nat. Mater.*, 2005, **4**, 366–377.
9 H. Duan, J. Gnanaraj, X. Chen, B. Li and J. Liang, *J. Power Sources*, 2008, **185**, 512–518.
10 S. Chou, F. Cheng and J. Chen, *Eur. J. Inorg. Chem.*, 2005, 4035–4039.
11 Y. Fan and R. Wang, *Adv. Mater.*, 2005, **17**, 2384–2388.
12 F. Bonet, C. Guery, D. Guyomard, R. Herrera Urbina, K. Tekaia-Elhsissen and J. M. Tarascon, *Solid State Ionics*, 1999, **126**, 337–348.
13 L. Zhang, Y. Zhang, X. Zhang, Z. Li, G. Shen, M. Ye, C. Fan, H. Fang and J. Hu, *Langmuir*, 2006, **22**, 8109–8113.
14 H. J. Liu, S. H. Bo, W. J. Cui, F. Li, C. X. Wang and Y. Y. Xia, *Electrochim. Acta*, 2008, **53**, 6497–6503.
15 Z. S. Wu, W. Ren, L. Wen, L. Gao, J. Zhao, Z. Chen, G. Zhou, F. Li and H. M. Cheng, *ACS Nano*, 2010, **4**, 3187–3194.
16 J. Zhu, T. Sun, J. Chen, W. Shi, X. Zhang, X. Lou, S. Mhaisalkar, H. H. Hng, F. Boey, J. Ma and Q. Yan, *Chem. Mater.*, 2010, **22**, 5333–5339.